

The molecular gas kinematics in the host galaxy of non-repeating FRB 180924B

Tzu-Yin Hsu,¹★ Tetsuya Hashimoto,² Bunyo Hatsukade,³ Tomotsugu Goto,⁴ Po-Ya Wang,¹ Chih Teng Ling,⁴ Simon C.-C. Ho,^{4,5} and Yuri Uno²

¹*Department of Physics, National Tsing Hua University, 101, Section 2, Kuang-Fu Road, Hsinchu, 30013, Taiwan (R.O.C.)*

²*Department of Physics, National Chung Hsing University, No. 145, Xingda Rd., South Dist., Taichung, 40227, Taiwan (R.O.C.)*

³*Institute of Astronomy, Graduate School of Science, The University of Tokyo, 2-21-1 Osawa, Mitaka, Tokyo 181-0015, Japan*

⁴*Institute of Astronomy, National Tsing Hua University, 101, Section 2, Kuang-Fu Road, Hsinchu, 30013, Taiwan (R.O.C.)*

⁵*Research School of Astronomy and Astrophysics, The Australian National University, Canberra, ACT 2611, Australia*

Accepted 2022 December 06. Received 2022 December 02; in original form 2022 October 20

ABSTRACT

Fast radio bursts (FRBs) are millisecond-duration transients with large dispersion measures. The origin of FRBs is still mysterious. One of the methods to comprehend FRB origin is to probe the physical environments of FRB host galaxies. Mapping molecular-gas kinematics in FRB host galaxies is critical because it results in star formation that is likely connected to the birth of FRB progenitors. However, most previous works of FRB host galaxies have focused on its stellar component. Therefore, we, for the first time, report the molecular gas kinematics in the host galaxy of the non-repeating FRB 180924B at $z = 0.3216$. Two velocity components of the CO (3-2) emission line are detected in its host galaxy with the Atacama Large Millimeter/submillimeter Array (ALMA): the peak of one component ($-155.40 \text{ km s}^{-1}$) is near the centre of the host galaxy, and another (-7.76 km s^{-1}) is near the FRB position. The CO (3-2) spectrum shows asymmetric profiles with $A_{\text{peak}} = 2.03 \pm 0.39$, where A_{peak} is the peak flux density ratio between the two velocity components. The CO (3-2) velocity map also indicates an asymmetric velocity gradient from -180 km s^{-1} to 8 km s^{-1} . These results indicate a disturbed kinetic structure of molecular gas in the host galaxy. Such disturbed kinetic structures are reported for repeating FRB host galaxies using HI emission lines in previous works. Our finding indicates that non-repeating and repeating FRBs could commonly appear in disturbed kinetic environments, suggesting a possible link between the gas kinematics and FRB progenitors.

Key words: (transients:) fast radio bursts – Galaxy: kinematics and dynamics – ISM: molecules – radio line: ISM – cosmology: observations

1 INTRODUCTION

Fast radio bursts (FRBs) are millisecond-duration, energetic, and highly dispersed radio pulses (Lorimer et al. 2007). Most of them are regarded as extragalactic transients due to their large dispersion measures (e.g., Thornton et al. 2013; Cordes & Chatterjee 2019) and localization to the host galaxies (e.g., Tendulkar et al. 2017; Bannister et al. 2019; Nimmo et al. 2022). FRBs include two types, repeating FRBs and non-repeating FRBs. Whether the two populations of FRBs originate from similar progenitors is still highly debated (e.g., Hashimoto et al. 2020; Pleunis et al. 2021). So far, there are more than 800 FRBs detected, and numerous models have been proposed

(e.g., Margalit & Metzger 2018; Kashiyama & Murase 2017; Lyutikov et al. 2016; Platts et al. 2019) to understand the progenitor of FRBs. However, the origin of FRBs remains a mystery. One of the methods to comprehend the origin of FRBs is to probe the physical environments of their host galaxy. Most previous studies of FRB host galaxies are mainly focusing on its stellar components (e.g., Bhandari et al. 2022; Mannings et al. 2021; Heintz et al. 2020). The optical work of Bhandari et al. (2022), which reported diverse properties of FRB host galaxies, suggests that there is no significant difference between the physical properties of host galaxies of repeating and non-repeating FRBs. The mass-weighted stellar-mass cumulative distributions in Bhandari et al. (2022) indicate that FRB host galaxies are less massive than typical star-forming galaxies with the p -value of $P_{KS} = 0.002$ for the Kolmogorov-Smirnov test.

★ E-mail: emma30407@gmail.com

HI-gas (molecular-gas) kinematics probed by radio (submillimeter) observations allows us to investigate variable physical processes of host galaxies (e.g., infalling gas, merger, and smooth rotation). The previous study of HI distribution in the host galaxy of repeating FRB 180926B (Kaur et al. 2022) indicates the disturbed and merging kinetic structure of HI gas. Kaur et al. (2022) argues that the merging gas caused the burst of star formation in the outskirts of the host galaxy, which might be linked to the progenitor activity. Asymmetric HI spectral shapes are reported for the host galaxies of repeating FRB 181030A, FRB 200120E, and FRB200428, indicating features of galaxy interactions (Michałowski 2021). The interactions found in these repeating FRB host galaxies indicate that there might be a connection between the birth of the FRB progenitors and recently enhanced star formation via interaction (Michałowski 2021).

Since stars are born from molecular gases, they provide us with a more direct probe of kinetic features and a recent enhancement of star formation than HI gas. Therefore, mapping molecular-gas kinematics with CO observations in FRB host galaxies is critical, and the kinematics gives rise/decline to recent star formation that is likely connected to the origins of two FRB populations: non-repeating and repeating FRBs. Although understanding molecular-gas kinematics provides an insightful perspective, it has been poorly understood so far. To overcome this problem, we, for the first time, investigate molecular-gas kinematics in a host galaxy of a non-repeating FRB 180924B to understand the progenitor environments with the Atacama Large Millimeter/submillimeter Array (ALMA).

Hatsukade et al. (2022) discussed the diverse molecular-gas properties in FRB host galaxies based on ALMA CO observations. The host galaxy of FRB 180924B is more gas-rich than the general star-forming galaxies (Hatsukade et al. 2022). They used a moderate velocity resolution of 50 km s^{-1} to enhance CO detection. In this work, we use the same data as used by Hatsukade et al. (2022) with a better velocity resolution of 9 km s^{-1} to focus on the kinematics of molecular gas. We report the first analysis of the kinetic structure of the molecular gas in the host galaxy of non-repeating FRB 180924B. The paper is organized as follows: In section 2, we present the ALMA data and data reduction. Section 3 demonstrates the kinetic structure in molecular gas. We discuss the possible environmental similarity in terms of gas kinematics between repeating FRBs and non-repeating FRBs in Section 4.

2 OBSERVATION AND DATA ANALYSIS

The observation of FRB 180924B was conducted with Australia Square Kilometre Array Pathfinder (ASKAP) on 2018 September 24 at 16:23:12.6265 UTC (Bannister et al. 2019). The host is a massive spiral galaxy at $z = 0.3214$ with a stellar mass of $M_* = (1.32 \pm 5.1) \times 10^9 M_\odot$ and the star formation rate (SFR) of $0.88 \pm 0.26 M_\odot \text{ yr}^{-1}$ (Bannister et al. 2019; Heintz et al. 2020). We utilized ALMA Science Archive data of Band 6 CO (3-2) observation of the FRB 180924B host galaxy with the project code 2019.01450.S¹. The host of FRB 180924B was observed using 44–46 antennas in array configuration with 15.0–311.7 m baseline length on November 26, 2019, for a total of 27 minutes on the source. The bandwidth of the correlator setup is 1.875 GHz, subsided into 240 channels.

The data reduction is conducted with Common Astronomy

Software Application (CASA; McMullin et al. 2007), and the calibration data is processed with the CASA pipeline version 5.6.1-8. The data cube is obtained with the CASA task `tclean()` by setting the robust parameter of 2.0 for Briggs weighting with a velocity resolution of $\sim 9 \text{ km s}^{-1}$. The observed frequency of the data cube is converted to the rest-frame frequency using the spectroscopic redshift of $z = 0.3214$ (Bannister et al. 2019). The Doppler velocity is calculated using the rest-frame frequency of the CO (3-2) emission line, i.e., 345.796 GHz. The velocity-integrated intensity (moment 0) map and the velocity structure (moment 1) map are obtained by Cube Analysis and Rendering Tool for Astronomy (CARTA) (Comrie et al. 2021). The synthesized beam of the two maps is $0''.51 \times 0''.68$.

3 RESULTS

3.1 CO emission line detection

Figure 1 (left) shows the velocity-integrated intensity map with the integration range of $\sim -180 \text{ km s}^{-1}$ to $\sim 110 \text{ km s}^{-1}$. The CO (3-2) emission line is significantly detected at the position of the host galaxy within two-times half-light radius (r_{half}): $r_{\text{half}} = 0.516 \text{ arcsec} \sim 2.5 \text{ kpc}$ (Bhandari et al. 2020). We utilize an aperture with a radius of 1.032 arcsec (5 kpc) centred at the host galaxy (RA, Dec) = (21h44m25.25s, $-40^\circ 54' 00.81''$) (Bhandari et al. 2020) to extract a CO spectrum of the host galaxy. Figure 1 (right) shows the extracted CO spectrum. In figure 1 (right), two velocity components are detected. We fit double Gaussian functions to these two components in the spectrum. The best-fit double Gaussian functions show the systematic velocities (V_{sys}) of $-155.40 \text{ km s}^{-1}$ and -7.76 km s^{-1} with velocity dispersions (σ_V) of 16 km s^{-1} and 58 km s^{-1} , respectively.

3.2 Positional offset between two peaks

Using the CASA task `imfit`, we obtain the central position of each peak of the two velocity components. The positional information and the physical properties of two velocity components are listed in table 1. The distance between the two peaks is $\sim 0''.51$, which is more than 5σ apart with the positional uncertainty (e) of $\sim 0''.10$ that is derived from the following equation:

$$e = \frac{a}{S/N}, \quad (1)$$

where a is the major axis of the beam size in arc second. Both $a \sim 0''.68$ and $S/N = 9.60$ and 8.76 (table 1) are obtained from the velocity-integrated intensity map in figure 2. We calculate a quadrature sum of the positional errors of the two velocity components to derive $\sim 0''.10$ positional uncertainty.

Figure 2 shows the velocity-integrated intensity map with contours of different flux levels of two velocity components. The map shows multiple spatial components, where the blue contour represents the first component with $V_{\text{sys}} = -155.40 \text{ km s}^{-1}$ while the red contour represents the second component with $V_{\text{sys}} = -7.76 \text{ km s}^{-1}$. Each velocity component is integrated over $\pm 2 \sigma_V$ from V_{sys} . The centre of the blue contour is relatively close to the FRB position, while the centre of the red contour is close to the host galaxy centre.

The CO luminosity and molecular gas mass are derived from the CO(3-2) emission-line flux measurement for each component.

¹ <https://www.youtube.com/watch?v=qz92y4AtpDo>

Table 1. Physical properties of each peak

Component	RA	Dec	V_{sys} (km s ⁻¹)	σ_V (km s ⁻¹)	S/N	L_{CO} (K km s ⁻¹ pc ²)	M_{gas} (M_{\odot})
Component 1	21h44m25.2650 ± 0.0034s	-40°54′01.0496″ ± 0.0271″	-155.40	16.40	9.60	(9.35 ± 0.97) × 10 ⁷	(7.31 ± 0.76) × 10 ⁸
Component 2	21h44m25.2511 ± 0.0037s	-40°54′00.5665″ ± 0.0394″	-7.76	58.60	8.76	(1.65 ± 0.18) × 10 ⁸	(1.28 ± 0.14) × 10 ⁹

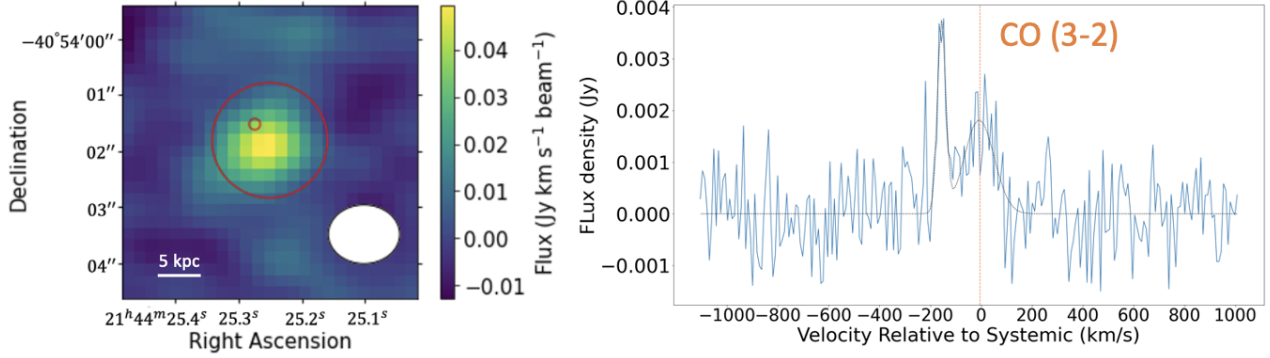


Figure 1. (left) CO velocity-integrated intensity map of the host galaxy of FRB 180924B. The velocity range from -180 to 110 km s⁻¹ is integrated. The large red circle indicates the position of the host galaxy with a radius of twice its half-light radius (Bhandari et al. 2020). The small red circle indicates the FRB position there with an error as its radius (Bannister et al. 2019). The beam size of ALMA data is shown by a white ellipse at the bottom right corner. (right) The spectrum of the CO emission line in the host galaxy of FRB 180924B. It is extracted from the aperture with a radius of $1.032''$ (5 kpc) centred at the host galaxy (large red circle in the left figure). The blue line shows the observed data, the black line shows the double-Gaussian fit to the data, and the orange dashed line represents the systemic velocity at $z = 0.3214$.

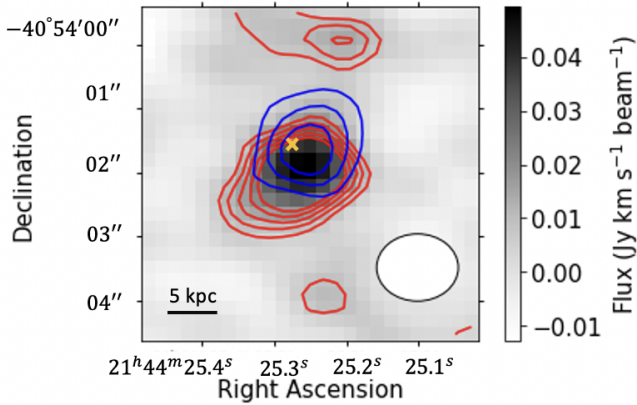


Figure 2. The positional offset between the two CO (3-2) emission-line components are overplotted on the velocity-integrated intensity map (figure 1) in grey scale. Blue and red contours indicate the flux level of the first (centred at -155.40 km s⁻¹ in figure 1) and second (centred at -7.76 km s⁻¹) velocity components, respectively. The centres of the contours are the position of two velocity components, which are present in table 1. The contour starts from 2.5σ level with 1σ increment. We note that all the contours are not drawn for clarity. The grey scale corresponds to the emission-line flux integrated over the velocity range from -180 km s⁻¹ to 110 km s⁻¹ that is extracted from the CO spectrum in figure 1. The yellow cross represents the position of FRB 180924B (Bannister et al. 2019).

The CO Luminosity is calculated using equation (3) in Solomon & Vanden Bout (2005) as follows:

$$L'_{\text{CO}(3-2)} = 3.25 \times 10^7 S_{\text{CO}(3-2)} \Delta V v_{\text{obs}}^{-2} D_L^2 (1+z)^{-3}, \quad (2)$$

where $L'_{\text{CO}(3-2)}$ is measured in K km⁻¹ s⁻¹ pc², $S_{\text{CO}(3-2)} \Delta V$ is the velocity integrated flux in Jy km s⁻¹, v_{obs} is the observed frequency of the CO(3-2) emission line in GHz, and D_L is the luminosity distance to the host galaxy in Mpc. The Molecular gas mass is derived as follows:

$$M_{\text{gas}} = \alpha_{\text{CO}} L'_{\text{CO}(1-0)}. \quad (3)$$

The CO (1-0) luminosity ($L'_{\text{CO}(1-0)}$) is derived by applying the CO luminosity ratio of $L'_{\text{CO}(3-2)}/L'_{\text{CO}(1-0)} = 0.55$ for star-forming galaxies (Lamperti et al. 2020; Hatsukade et al. 2022). The conversion factor α_{CO} is regarded as related to the gas-phase metallicity. The increasing α_{CO} indicates the decreasing gas-phase metallicity (Bolatto et al. 2013). We adopted $\alpha_{\text{CO}} = 4.3 M_{\odot} (\text{K km}^{-1} \text{s}^{-1} \text{pc}^2)^{-1}$ since the gas-phase metallicity is $12 + \log(\text{O}/\text{H}) = 8.93 \pm 0.02$ (Heintz et al. 2020), which is comparable to the Milky way gas-phase metallicity.

The CO luminosity and molecular gas mass of each peak are demonstrated in Table 1. The total CO luminosity (molecular-gas mass) of the two velocity components is $(2.59 \pm 0.20) \times 10^8$ K km s⁻¹ pc² ($(2.01 \pm 0.16) \times 10^9 M_{\odot}$). This value is consistent with $(3.1 \pm 0.3) \times 10^8$ K km s⁻¹ pc² ($(2.4 \pm 0.2) \times 10^9 M_{\odot}$) reported by (Hatsukade et al. 2022) within the errors.

3.3 Asymmetric CO spectrum

The right panel of figure 1 shows the asymmetric profile of the CO(3-2) spectrum, which could indicate the disturbed kinetic structure of molecular gas. To test the asymmetry of the CO spectrum, we apply the diagnostic (Reynolds et al. 2020) to define the spectrum asymmetry, deriving the ratio of the integrated fluxes between the

Table 2. Comparison of asymmetry parameters with different galaxies (Michałowski 2021)

Host galaxy	A_{flux}	A_{peak}
FRB 180924B	1.05 ± 0.16	2.03 ± 0.39
FRB 181030A	1.314 ± 0.072	1.505 ± 0.084
FRB 200120E	1.505 ± 0.002	1.551 ± 0.004
GRB 980425	1.027 ± 0.066	1.112 ± 0.071
GRB 111005A	1.237 ± 0.102	1.314 ± 0.104
LVHIS	1.110 ± 0.070	1.100 ± 0.090
HALOGAS	1.070 ± 0.050	1.110 ± 0.110
VIVA	1.190 ± 0.170	1.200 ± 0.210

left and right half of the spectrum, A_{flux} (equation 6 in Reynolds et al. 2020) and the peak ratio of the two velocity components, A_{peak} (equation 7 Reynolds et al. 2020). To derive A_{flux} , the boundary between the left and right half of the spectrum is defined by the mid-point of the full width at 20 % of the maximum peak height as V_{mid} . We also define the velocity that increases to the 20 % of peak flux density in the first component as V_{low} and the velocity that decreases to the 20 % of peak flux density in the second component as V_{high} . We integrate the best-fit Gaussian function from V_{low} to V_{mid} for the left half and V_{mid} to V_{high} for the right half. If A_{flux} or $A_{\text{peak}} < 1$, we take the inverse values such that both A_{flux} and A_{peak} are higher than 1.

We compare our results with the asymmetry parameters of the HI emission lines in previous works, i.e., the host galaxy of FRB 181030A, FRB200120E, the host galaxy of long gamma-ray burst (GRB) GRB 980425 and GRB 111005A (Michałowski 2021), the galaxies with stellar masses of $9 < \log(M_{\text{star}}/M_{\odot}) < 10$ in Local Volume HI Survey (LVHIS), Hydrogen Accretion in Local Galaxies Survey (HALOGAS), and VLA Imaging of Virgo in Atomic Gas (VIVA) (Michałowski 2021; Koribalski et al. 2018; Chung et al. 2009; Heald et al. 2011). Figure 3 and table 2 shows the comparison of the asymmetry parameters. A_{flux} and A_{peak} of the FRB 180924B host are 1.05 ± 0.16 and 2.03 ± 0.39 , respectively. The high value of A_{peak} indicates significant asymmetry in the CO spectrum and the disturbed kinetic structure of molecular gas. Following Reynolds et al. (2020), we define the spectrum as asymmetry with $A_{\text{flux}} > 1.05$, which is commonly used in the early studies (e.g., Reynolds et al. 2020). The comparison sample by Michałowski (2021) also uses 1.05, allowing a fair comparison with previous studies. A_{flux} of the host galaxy of FRB 180924B is on the boundary of the asymmetry, whereas A_{peak} indicates the clear asymmetric kinematics. This might be because the kinetic information could be lost by the integration process (equation 6 in Reynolds et al. 2020), making A_{flux} less sensitive to the spectral shape of FRB 180924B host. Furthermore, figure 4 shows the velocity field of the region with CO (3-2) emission-line detection higher than 4σ . The velocity map indicates a smooth velocity gradient from $\sim -180 \text{ km s}^{-1}$ to $\sim 8 \text{ km s}^{-1}$. The missing positive velocity component indicates the asymmetric velocity gradient, suggesting a disturbed kinetic structure of molecular gas instead of a smooth and symmetric rotation.

4 DISCUSSION AND CONCLUSION

To understand the gas kinematics in repeating and non-repeating FRB hosts, we compare our result of non-repeating FRB host with the previous study of HI detection (Kaur et al. 2022; Michałowski 2021) of repeating FRB host galaxies. However, we note that the HI and H_2 gas do not necessarily trace each other or are not necessarily physically associated. Therefore, the following comparison between the HI kinematics of the repeating FRB host galaxy and molecular gas kinematics is not strictly direct. The host galaxy of repeating FRB 20180916B (Kaur et al. 2022) shows a distorted and merging kinetic structure of HI gas which is experiencing a minor merger. The merging gas increases the HI mass and leads to the burst of star formation in the outskirts of the host galaxy, suggesting a possible link between the FRB progenitor and the enhanced star formation (Kaur et al. 2022).

In Michałowski (2021), the asymmetric HI spectra of repeating FRB host galaxies i.e., NGC 3252 (the host of FRB 181030A) and M81 (the host of FRB 200120E), show the disturbed HI gas structures, resulting in the recent enhancement of SFR due to the interaction between galaxies. However, the environment of FRB 200120E is puzzling because the FRB is localized in a globular cluster in M81 (Kirsten et al. 2022), which is an old system in contrast to the enhanced SFR due to the gas interaction.

In our work, the asymmetric CO spectrum (figure 1 right), the multiple spatial components in the velocity integrated intensity map (figure 2), and the asymmetric velocity gradient in velocity structure (figure 4) all indicate the disturbed kinematic structure of molecular gas in the host galaxy. A comparison to the previous works (Kaur et al. 2022; Michałowski 2021) suggests that the disturbed kinetic gas structure could commonly appear in both repeating and non-repeating FRB, which suggests a possible link between the gas kinematics and the FRB progenitors.

Previous optical studies found that FRB host galaxies show diverse properties in the colour-magnitude diagram and BPT diagram (Heintz et al. 2020; Bhandari et al. 2022), implying no conclusive answer to the galaxy population of FRB hosts. Our study reveals a new perspective that disturbed gas kinematics are found in both repeating and non-repeating FRB host galaxies and suggests the possible link to their progenitors. However, the observation of molecular gas in FRB host galaxies is still limited. Therefore, more observations are essential to understand the relationship between the gas kinematics and FRB progenitor.

ACKNOWLEDGEMENTS

We are very grateful to the anonymous referee for insightful comments. We thank the ALMA staff for data acquisition and Casa technical manipulation. T-YH acknowledges the University Consortium of ALMA-Taiwan Center for ALMA Science Advancement through a grant 110-2112-M-007-034-. TH acknowledges the support of the National Science and Technology Council of Taiwan through grants 110-2112-M-005-013-MY3, 110-2112-M-007-034-, and 111-2123-M-001-008-. TG acknowledges the support of the National Science and Technology Council of Taiwan through grants 108-2628-M-007-004-MY3 and 111-2123-M-001-008-. BH is supported by JSPS KAKENHI Grant Number 19K03925. This paper makes use of the following ALMA data: ADS/JAO.ALMA#2019.1.01450.S. ALMA is a partnership of ESO (representing its member states), NSF (USA) and NINS (Japan), together with NRC (Canada), MOST and ASIAA (Taiwan), and KASI

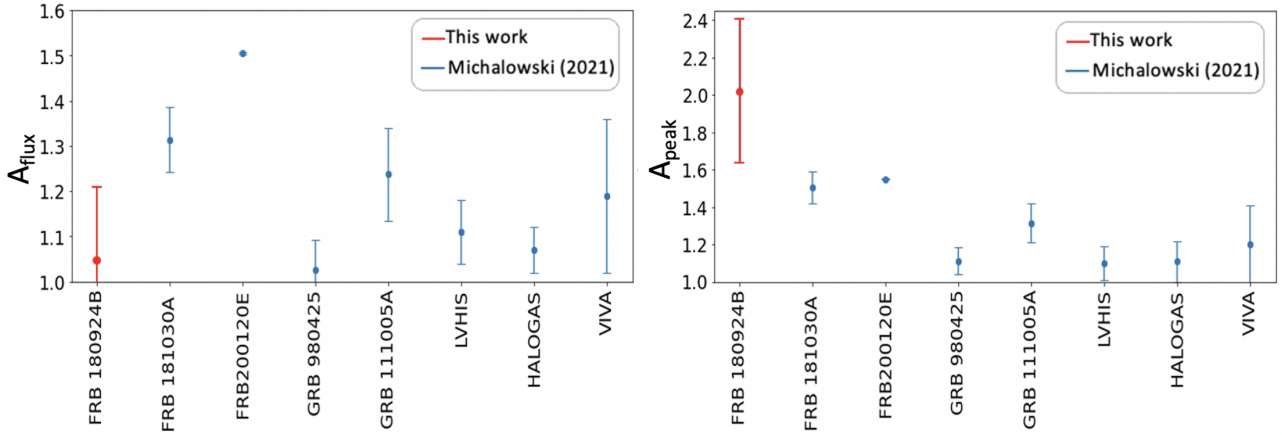


Figure 3. Asymmetry diagnostics: (left) the ratio of the integrated fluxes between the left and right half of the spectrum, A_{flux} , with the boundary defined by the mid-point of the full width at 20 % of the maximum peak height as V_{mid} . The velocity that increases to the 20 % of peak flux density in the first component is defined as V_{low} and the velocity that decreases to the 20 % of peak flux density in the second component is defined as V_{high} . We integrate the best-fit Gaussian function from V_{low} to V_{mid} for the left half and V_{mid} to V_{high} for the right half. (right) the ratio of the flux densities of the two peaks. The asymmetry parameter is compared with the FRB host galaxies, GRB host galaxies, and galaxy survey, i.e., LVHIS, HALOGAS, and VIVA (Michalowski 2021). Compared with other galaxies, FRB180924B host galaxy shows high A_{peak} . If A_{peak} or $A_{\text{flux}} < 1$, we take the inverse value.

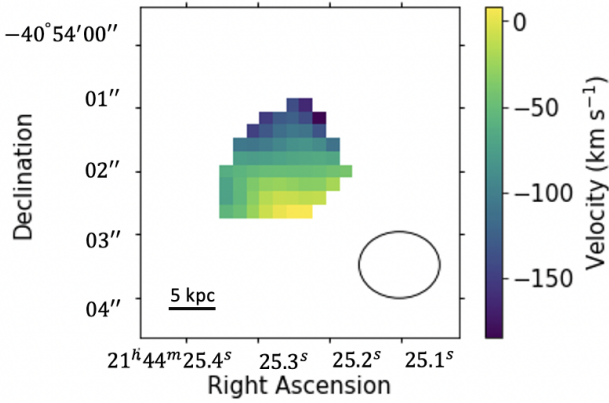


Figure 4. Velocity map of the CO (3-2) emission of the FRB 180924B host. The region is chosen for the CO emission higher than 4σ . The colours indicate molecular gas velocities at different positions. An ellipse shows the beam size of ALMA data at the bottom right corner.

(Republic of Korea), in cooperation with the Republic of Chile. The Joint ALMA Observatory is operated by ESO, AUI/NRAO, and NAOJ.

DATA AVAILABILITY

The data underlying this article can be obtained through ALMA Science Archive (<https://almascience.nrao.edu/aq/>).

REFERENCES

- Bannister K. W., et al., 2019, *Science*, 365, 565
 Bhandari S., et al., 2020, *ApJ*, 895, L37
 Bhandari S., et al., 2022, *AJ*, 163, 69
 Bolatto A. D., Wolfire M., Leroy A. K., 2013, *ARA&A*, 51, 207

- Chung A., van Gorkom J. H., Kenney J. D. P., Crowl H., Vollmer B., 2009, *The Astronomical Journal*, 138, 1741
 Comrie A., et al., 2021, CARTA: Cube Analysis and Rendering Tool for Astronomy, Astrophysics Source Code Library, record ascl:2103.031 (ascl:2103.031)
 Cordes J. M., Chatterjee S., 2019, *ARA&A*, 57, 417
 Hashimoto T., Goto T., Wang T.-W., Kim S. J., Ho S. C. C., On A. Y. L., Lu T.-Y., Santos D. J. D., 2020, *MNRAS*, 494, 2886
 Hatsukade B., Hashimoto T., Niino Y., Hsu T.-Y., 2022, *The Astrophysical Journal Letters*, 940, L34
 Heald G., et al., 2011, *A&A*, 526, A118
 Heintz K. E., et al., 2020, *ApJ*, 903, 152
 Kashiyama K., Murase K., 2017, *ApJ*, 839, L3
 Kaur B., Kanekar N., Prochaska J. X., 2022, *ApJ*, 925, L20
 Kirsten F., et al., 2022, *Nature*, 602, 585
 Koribalski B. S., et al., 2018, *MNRAS*, 478, 1611
 Lamperti I., et al., 2020, *ApJ*, 889, 103
 Lorimer D. R., Bailes M., McLaughlin M. A., Narkevic D. J., Crawford F., 2007, *Science*, 318, 777
 Lyutikov M., Burzawa L., Popov S. B., 2016, *MNRAS*, 462, 941
 Mannings A. G., et al., 2021, *ApJ*, 917, 75
 Margalit B., Metzger B. D., 2018, *The Astrophysical Journal*, 868, L4
 McMullin J. P., Waters B., Schiebel D., Young W., Golap K., 2007, in Shaw R. A., Hill F., Bell D. J., eds, *Astronomical Society of the Pacific Conference Series Vol. 376, Astronomical Data Analysis Software and Systems XVI*. p. 127
 Michalowski M. J., 2021, *ApJ*, 920, L21
 Nimmo K., et al., 2022, *The Astrophysical Journal Letters*, 927, L3
 Platts E., Weltman A., Walters A., Tendulkar S. P., Gordin J. E. B., Kandhai S., 2019, *Phys. Rep.*, 821, 1
 Pleuniz Z., et al., 2021, *ApJ*, 923, 1
 Reynolds T. N., Westmeier T., Staveley-Smith L., Chauhan G., Lagos C. D. P., 2020, *MNRAS*, 493, 5089
 Solomon P. M., Vanden Bout P. A., 2005, *ARA&A*, 43, 677
 Tendulkar S. P., et al., 2017, *ApJ*, 834, L7
 Thornton D., et al., 2013, *Science*, 341, 53

This paper has been typeset from a \LaTeX file prepared by the author.